Journal of Physics and Chemistry of Solids 85 (2015) 69–74

Contents lists available at ScienceDirect

Journal of Physics and Chemistry of Solids

journal homepage: www.elsevier.com/locate/jpcs

Heat capacity, thermal expansion and heat transport in the Han Blue ($BaCuSi_4O_{10}$): Observation of structural phase transitions

S.H. Masunaga [a], A. Rebello [a], A.T. Schye [a], N. Prasai [b], J.J. Neumeier [a,*], J.L. Cohn [b]

[a] Physics Department, P.O. Box 173840, Montana State University, Bozeman, MT 59717-3840, USA
[b] Department of Physics, University of Miami, Coral Gables, FL 33124, USA

ARTICLE INFO

Article history:
Received 11 November 2014
Received in revised form
22 April 2015
Accepted 30 April 2015
Available online 4 May 2015

Keywords:
Optical materials
Crystal structure
Thermal expansion
Specific heat
Thermal conductivity

ABSTRACT

Structural phase transitions at 87 K and 103 K are reported for single-crystalline Han Blue ($BaCuSi_4O_{10}$) by means of high-resolution thermal-expansion, thermal conductivity and heat capacity measurements. The phase transition at 103 K results in differing lengths of the *a* and *b* lattice parameters, and thus a lowering of the crystallographic symmetry. Negative thermal-expansion coefficients are observed perpendicular to the *c*-axis over a wide temperature range (108 K < T < 350 K). The thermal conductivity is small, and decreases with temperature, both of which suggest strong scattering of heat-carrying phonons. The principle Grüneisen parameter within the plane and perpendicular to it was determined to be $\gamma_1 = -1.09$ and $\gamma_3 = 1.06$ at room temperature; the bulk Grüneisen parameter is $\gamma = 0.10$. The results are consistent with the presence of low-energy vibrations associated with the collective motions of CuO_4 and Si_4O_{10} polyhedral subunits.

1. Introduction

$BaCuSi_4O_{10}$ was used in many Chinese artifacts as a synthetic pigment. It was named Han Blue by FitzHugh and Zycherman [1]. The stable blue color is rare in nature; therefore, the chemical development and the production of blue pigments began in ancient times with Egyptian Blue ($CaCuSi_4O_{10}$) in Egypt and Han Blue ($BaCuSi_4O_{10}$) and Han Purple ($BaCuSi_2O_6$) in China [2]. Besides being important synthetic pigments of ancient and modern times, Egyptian Blue and Han Blue have attracted scientific and technological interest due to their extraordinary luminescent properties [3–5]. Their crystal structures differ, in that Han Blue possesses silicate layers while Han Purple contains isolated Si_4O_{12} rings [6], leading to isolated Cu_2 dimers [7,8]. A gapped spin dimer ground state exists in Han Purple, which displays Bose–Einstein condensation in strong magnetic field [9]. No such state is known to exist in the Han Blue.

The room temperature crystal structure of Han Blue and its corresponding rare mineral effenbergerite is tetragonal, space group P4/ncc (130), with $a = 7.447(1)$ Å, $c = 16.138(2)$ Å, and $Z = 4$ at 300 K. It consists of a two-dimensional network of condensed silicate tetrahedrons, which contains four-member rings of SiO_4 tetrahedral units connected to other inverted rings by apical oxygen to form Si_8O_{20} sheets. The rings are linked together by square-planar coordinated copper, forming double copper-silicate $[CuSi_4O_{10}]_n$ layers parallel to the (001) plane, which are joined by barium ions that are positioned between these layers. The blue color of $BaCuSi_4O_{10}$ compounds comes from crystal-field splitting of the Cu^{2+} *d* orbitals in their square-planar coordination [6,10,11].

The electronic, optical and structural properties of $BaCuSi_4O_{10}$ have been well investigated in the room temperature region [5,6,10–14]. Further knowledge of the physical properties may prove valuable due to increasing technological interest. In this work, high-resolution thermal expansion, thermal conductivity, heat capacity and magnetic susceptibility measurements of single crystalline Han Blue are reported. Although no structure phase transition was observed for the closely related compound $Ba_{0.5}Sr_{0.5}CuSi_4O_{10}$, that is isostructural with Han Blue and studied between 5 K and 300 K by neutron diffraction [15], our measurements reveal structural phase transitions at 87 K and 103 K. The transitions result in a lowering of the crystallographic symmetry from tetragonal, perhaps to orthorhombic or a lower symmetry. The change in the lattice parameters associated with this transition would be about one part in a few thousand, and could easily be missed in typical diffraction experiments. The high resolution of our thermal expansion technique, capable of observing changes in length of one part in 10^8, makes the transition readily visible. The negative thermal expansion, behavior of the thermal conductivity and heat capacity, and the Grüneisen parameters are consistent with the presence of low-energy vibrations associated with the collective motions of the CuO_4 and Si_4O_{10} polyhedral subunits. A steep increase of heat capacity below 2 K, characteristic of Schottky anomaly, is also observed.

* Corresponding author. Fax: +1 406 994 4452
E-mail address: neumeier@physics.montana.edu (J.J. Neumeier).

http://dx.doi.org/10.1016/j.jpcs.2015.04.021
0022-3697/

2. Experimental procedure

$BaCuSi_4O_{10}$ single crystals were grown using the flux-growth technique. Polycrystalline powder of $BaCuSi_2O_6$ was mixed with $LiBO_2$ in the molar proportion 2:1, and single phase $BaCuSi_4O_{10}$ crystals formed when the mixture was slow cooled, from 1200 °C to 875 °C at 1 °C/h. A faster cooling rate of 5 °C/h resulted in a mixture of $BaCuSi_2O_6$ and $BaCuSi_4O_{10}$ phases. The $BaCuSi_4O_{10}$ single crystals form platelets with [001] crystallographic direction perpendicular to the platelet plane. The single phase nature of the single crystals was confirmed by x-ray powder diffraction (not shown) after powdering some crystals. A preferential {00l} orientation was observed in the diffraction pattern due to the perfect cleavage of the crystals parallel to these planes. Three samples were oriented for the measurements using x-ray Laue diffraction with typical dimensions of about $2 \times 1.5 \times 0.5$ mm^3.

Magnetization and heat capacity measurements were performed using a Quantum Design Physical Property Measurement System (PPMS) equipped with a vibrating sample magnetometer (VSM). The magnetic field of $\mu_0 H = 0.5$ T was applied parallel and perpendicular to the c-axis in the 2–350 K temperature range; μ_0 is the permeability of free space. Heat capacity was measured in the 0.35–300 K temperature range using the thermal-relaxation technique. High-resolution thermal-expansion measurements were performed along the a-, b- and c-axes in a capacitive dilatometer cell constructed from fused quartz, with a sensitivity to length changes of $\Delta L = 0.1$ Å. The data were collected on heating, using a warming rate of 0.20 K/min. Details of this technique can be found elsewhere [16]. In the temperature range of 5–80 K, a piecewise Chebyshev polynomial fit of the linear thermal expansion ($\Delta L/L_{300\,K}(T)$) was performed before taking the point-by-point derivative to determine the linear thermal-expansion coefficient ($\mu(T)$), where $L_{300\,K}$ is the length of the sample at 300 K. Thermal conductivity was measured perpendicular to the c-axis in a radiation-shielded vacuum probe using a standard steady-state method with a temperature gradient produced by a chip heater and monitored by a 25 μm-diameter chromel–constantan differential thermocouple. Heat losses via radiation and conduction through leads were determined in separate experiments and the data corrected accordingly. This correction was 10–15% near room temperature and ≤3% for $T \leq 120$ K.

3. Results and discussion

The magnetic susceptibility $\chi(T)$ for the Han Blue crystal is shown in Fig. 1. There is some anisotropy in $\chi(T)$ measured with the magnetic field parallel and perpendicular to the c-axis. Han Blue is paramagnetic in the entire temperature range of the measurement, from 2 to 350 K, due to the isolated copper ions in the structure. A spin-only Curie–Weiss susceptibility [17] given by

$$\chi(T) = \frac{\mu_0 g^2 S(S+1)\mu_B^2 N_v}{3k_B(T-\theta)} + \chi_0, \quad (1)$$

was used to analyze the $\chi(T)$ data. Here, μ_0 is the permeability of free space, g the g-factor, μ_B the Bohr magneton, S the total spin, N_v the number of moments per unit volume, k_B the Boltzmann constant, T the temperature, θ the Curie–Weiss temperature, and χ_0 a temperature-independent contribution (due to Van Vleck and diamagnetic susceptibilities). In addition to the curves shown in Fig. 1, data were acquired on additional crystals and multiple directions within the plane; no anisotropy of χ was observed in the plane. The data were fitted to Eq. (1) for $T > 100$ K; for this temperature range and our magnetic field B, $gS\mu_B B/k_B T < 4 \times 10^{-3}$, which is within the range of validity for the Curie–Weiss

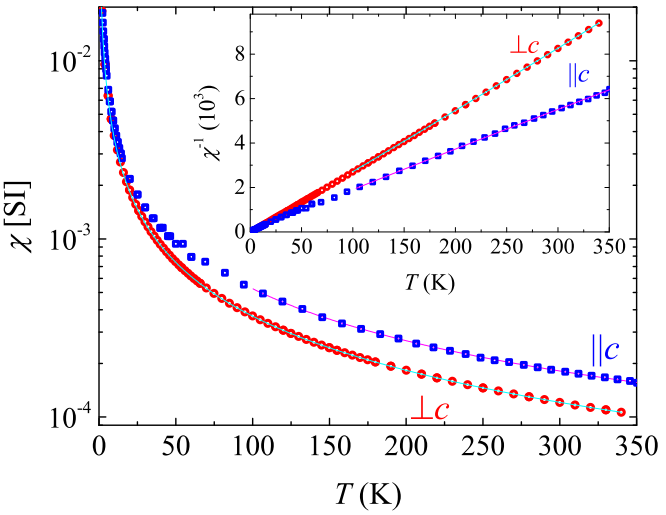

Fig. 1. Magnetic susceptibility for $BaCuSi_4O_{10}$. The data are plotted on a logarithmic scale to show the small anisotropy between the two curves, measured parallel and perpendicular to the c-axis. Solid lines are the fits using Eq. (1). The inset shows data plotted as χ^{-1} versus T, along with the fits using Eq. (1).

approximation. Values for χ_0 were found to range between 1.0×10^{-5} and 1.8×10^{-5} (in dimensionless SI units), yielding $\chi_0 = 1.3(5) \times 10^{-5}$. The diamagnetic susceptibility is estimated to be $\chi_{dia} = -1.6 \times 10^{-5}$ [18], leading to a temperature-independent paramagnetic susceptibility of $\chi_{para} = 2.9(5) \times 10^{-5}$. The Van Vleck contribution is estimated using [19] $\chi_{VV} = 4N_A\mu_B^2/E$, where N_A is Avogadro's number and $E = 16{,}500\ \mathrm{cm}^{-1}$ from Ref. [13], or $E = 12{,}600\ \mathrm{cm}^{-1}$ from Ref. [19]. The obtained values of χ_{VV} range from 6.0×10^{-6} to 7.8×10^{-6}, revealing that χ_{VV} accounts for only 20–27% of χ_{para}. Although this might suggest the presence of another paramagnetic contribution to χ, the discrepancy could reside with the value of χ_{dia}, which should only be taken as an estimate [17]. Corrections associated with the silicate layering of Han Blue are likely necessary to provide a more trustworthy estimate for χ_{dia}; this issue does not affect the remainder of our analysis. A value $\theta = -2(3)$ K was obtained, based on five independent measurements. Anisotropic g-factors with $g = 2.41(7)$ and 2.09(5) were obtained for $\chi(T)$ measured under magnetic field parallel and perpendicular to the c-axis, respectively, in agreement with values calculated from electronic structure of Cu^{2+} in Han Blue [13]. The corresponding effective magnetic moments are μ_{eff} of 2.1 μ_B and 1.8 μ_B, respectively, where $\mu_{eff} = g\sqrt{S(S+1)}\mu_B$; these are in accord with expected [20] values for Cu^{2+}.

The temperature dependence of the linear thermal expansion $\Delta L/L_T$, where $\Delta L = L(T) - L_T$ and L_T is the sample length at temperature T, measured along the principal crystallographic directions, is shown in Fig. 2. Significant anisotropy is evident. The sample expands along c with increasing temperature for $T > 5$ K with an overall variation in $\Delta L/L_{300\,K}$ between 5 K and 300 K of 3.39×10^{-3}. This is more than three times larger than the maximum variation in the perpendicular direction (i.e. within the a–b plane). In this direction, it expands from 5 K to 108 K, and then changes behavior, contracting for $T > 108$ K. The resulting overall variation of $\Delta L/L_{300\,K}$ between 5 K and 300 K is very small, with values of 0.19×10^{-3} and 0.49×10^{-3} along a and b, respectively. The maximum variation along these respective directions (0.80×10^{-3} and 1.07×10^{-3}), however, occurs below 108 K. Above 108 K, Han Blue contracts along a and b and expands along c with increasing T. This behavior leads to a very small volume thermal expansion $\Delta V/V_{300\,K}$ (see the inset of Fig. 2(a)) above 108 K, which was approximated by $\Delta V/V_T = \Delta L_a/L_T^a + \Delta L_b/L_T^b + \Delta L_c/L_T^c$, where

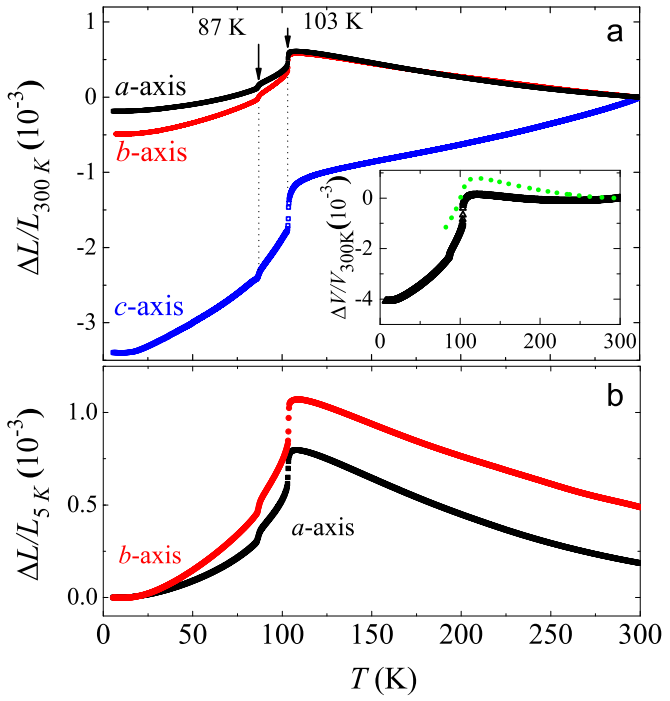

Fig. 2. (a) Linear thermal expansion $\Delta L/L_{300\,K}$ for $BaCuSi_4O_{10}$ along the indicated axes. The inset shows the volume thermal expansion $\Delta V/V_{300\,K}$ for single crystal (black symbols) and polycrystal (green dotted line, above 82 K). (b) $\Delta L/L_{5\,K}$ for the *a*- and *b*-axes provides a different perspective due to the normalization at 5 K. (For interpretation of the references to color in this figure caption, the reader is referred to the web version of this paper.)

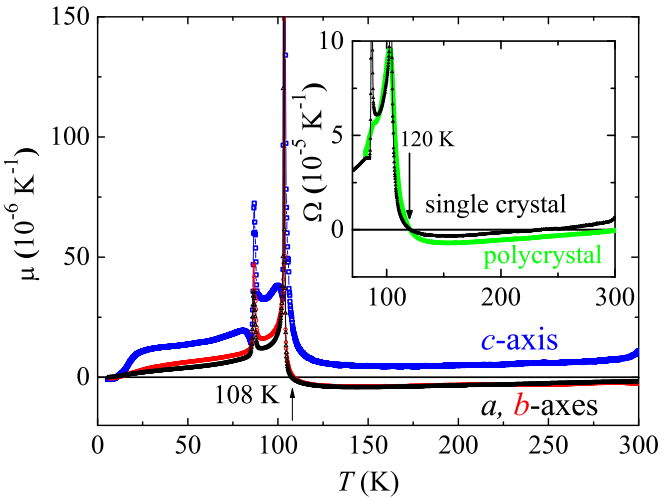

Fig. 3. Linear thermal-expansion coefficient $\mu(T)$ parallel and perpendicular to the *c*-axis for $BaCuSi_4O_{10}$. The inset shows the volume thermal-expansion coefficient $\Omega(T)$ for single crystal (line+symbol) and polycrystal (green solid line for $T>$ 82 K). (For interpretation of the references to color in this figure caption, the reader is referred to the web version of this paper.)

$\Delta L_a/L_T^a$, $\Delta L_b/L_T^b$ and $\Delta L_c/L_T^c$ are the linear thermal expansions along the *a*-, *b*- and *c*-axes, respectively, normalized to the length at *T*.

The abrupt change in $\Delta L/L_{300\,K}$ and $\Delta V/V_{300\,K}$ at 87 K and 103 K reveals that two successive structural phase transitions occur in $BaCuSi_4O_{10}$. The transitions are more visible in Fig. 2(b), where $\Delta L/L_{5\,K}$ for *a* and *b* are shown. Since it is well known that Han Blue is tetragonal at 300 K, and $\Delta L/L_{300\,K}$ along *a* and *b* overlap from 103 K to 300 K, the tetragonal phase is stable for the range 103 K $<T<$ 300 K, within the resolution of our experiments. The data illustrate that Han Blue undergoes a transition at 103 K to a structure with lower symmetry whereby the *a* and *b* lattice parameters are no longer equal. Two additional single crystals were measured from 82 K to 300 K; they exhibited results identical to those shown in Fig. 2.

One might surmise that the low-temperature phase is orthorhombic, but our thermal expansion measurements are unable to determine this. Furthermore, the transition at 87 K, which continues the trend of an increasing difference between the *a* and *b* lattice parameters upon cooling, could be caused by a further reduction in crystallographic symmetry. High-resolution diffraction experiments would be required to fully investigate the crystallographic changes at 103 K and 87 K. However, it is important to mention that the small crystallographic distortion between *a* and *b* of $\Delta L/L_T \sim 5\times10^{-4}$ would be challenging to study with the relative resolution afforded by x-ray or neutron diffraction.

Since abrupt changes in $\Delta L/L_T$ are observed, the transitions are first order because they correspond to discontinuities in the first derivative of the Gibbs free energy [21]. Generally, structural transitions are first order in nature. Further analysis is possible by calculating the linear thermal-expansion coefficient μ and the volume thermal-expansion coefficient Ω, which were determined using

$$\mu(T) = \frac{\partial}{\partial T}\left(\frac{\Delta L}{L_{300\,K}}\right), \tag{2}$$

and

$$\Omega(T) = \frac{\partial}{\partial T}\left(\frac{\Delta V}{V_{300\,K}}\right), \tag{3}$$

respectively. The resulting data are shown in Fig. 3. The first-order nature of the phase transitions at 87 K and 103 K are also inferred [21] by the large peaks in μ. Within the *a*–*b* plane, the values of μ remain equivalent only when $T>103$ K, again indicating that the tetragonal structure is not maintained below 103 K. For $T>$ 108 K, μ is negative, signifying that the sample contracts within the plane upon warming. Along the *c* direction, $\mu(T)$ is positive over the entire temperature range.

Summation of the three $\mu(T)$ curves yields the volume thermal expansion coefficient $\Omega(T)$, which is negative for the range 120 K $<T<$ 235 K, with a minimum value of $\approx -3.5\times10^{-6}$ K^{-1} (see the inset of Fig. 3). The small volume thermal-expansion coefficient for $T>$ 120 K is due to the opposite behavior between μ parallel and perpendicular to the *c*-axis. At 300 K, μ is 7.05×10^{-6} K^{-1} along the *c*-axis, -1.76×10^{-6} K^{-1} within the plane and $\Omega=3.53\times10^{-6}$ K^{-1}. The small volume thermal expansion near 300 K may be important to consider for technological applications, as pointed out in Ref. [22].

The insets of Figs. 2 and 3 show $\Delta V/V_{300\,K}$ and $\Omega(T)$, respectively, for polycrystalline Han Blue (above 82 K) plotted along with data from the single crystal. Qualitatively, the behavior of both curves is similar. However, the features at 87 K and 103 K are significantly broader in the polycrystal. Negative thermal expansion is observed in $\Omega(T)$ above 120 K, and it increases in a linear fashion above ~170 K for both specimens. However, their magnitudes are different for $T>$ 120 K. In the linear region, $\Omega(T)$ for the single crystal is 3.5×10^{-6} K^{-1} larger than that of the polycrystal. Therefore, Ω is negative over a wider temperature range for the polycrystal (120 K $<T<$ 310 K) than for the single crystal (120 K $<T<$ 240 K). The thermal expansion was measured along the directions parallel and perpendicular to the uniaxial pressure (*P*) applied to pelletize the polycrystalline sample. A small preferential direction effect was observed; when Ω was measured parallel to *P* it is ~0.8×10^{-6} K^{-1} larger than the Ω value found when it is measured perpendicular

to P for $T > 170$ K. However, this effect does not explain the observed difference between the single crystal and polycrystal data. Thus, it may be attributed to a variety of effects including a small preferential orientation, the difference in morphology of both samples (density and porosity), and internal strain.

High anisotropy in thermal expansion and negative thermal expansion are common in layered compounds [23]. It results from anisotropic bonding between atoms, with strong bonds within the layers and weaker bonding between layers. The differing bonding strengths influence the phonon modes and their associated anharmonicity. Weak bonding between neighboring layers results in low frequency phonon modes in this direction that are readily excited by thermal energy, thereby leading to large positive thermal expansion [24]. Perpendicular to the layers, stiff bonding leads to high frequency phonon modes. Thus, the low-frequency modes can dominate at low temperature, which causes tensile stress within the planes and the existence of bending modes [25]. Similar physics is certainly in play for the Han Blue, where intralayer bonds (Si–O) are much stronger than interlayer (Ba–O) bonds. This leads to a large thermal expansion along c and a smaller, sometimes negative, thermal expansion within the plane.

The thermal conductivity $\kappa(T)$ measured along the a- and b-axes of the same crystal is shown in Fig. 4 for the range 5 K $\leq T \leq$ 300 K. Crystals were too small to measure $\kappa(T)$ along c. The difference in the magnitudes of κ_a and κ_b in the tetragonal phase at $T \geq$ 103 K is within the uncertainty of the measurement (~20% due to the geometric factor). The most notable features of the data are the relatively small magnitude, κ(300 K) ~ 3 W/mK, and the continuous decrease in κ with decreasing T. Both features indicate strong scattering of heat-carrying phonons throughout the temperature range. A prominent anomaly is observed at 103 K associated with the structural transition, and a smaller feature is evident near 87 K where $\mu(T)$ has a clear anomaly. $\kappa(T)$ for both directions exhibits hysteresis in the range 82–87 K associated with the second transition, with cooling data lower in magnitude by ~1%. These data were taken with stabilized temperatures in 0.5 K steps. The hysteresis implies a coexistence of two structural configurations in the narrow transition region (e.g. involving distortions of molecular units), the volume fraction of which differ upon cooling and warming, thus leading to different scattering of the heat-carrying phonons. The presence of hysteresis suggests that the phase transition is first order. The overall T dependence is

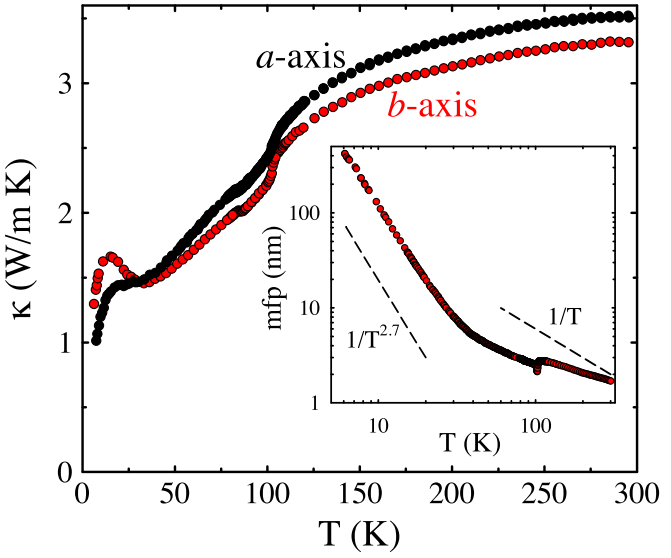

Fig. 4. Temperature dependence of thermal conductivity $\kappa(T)$ for the a- and b-axes of $BaCuSi_4O_{10}$. The inset shows the temperature dependence of the phonon mean free path (mfp).

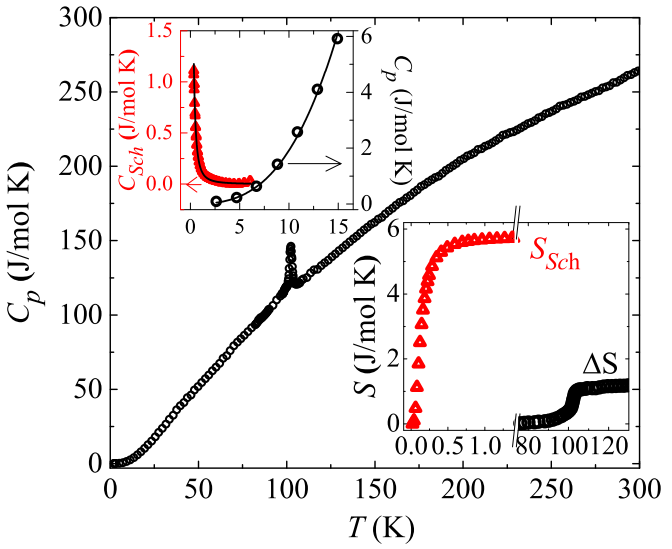

Fig. 5. Temperature dependence of specific heat for $BaCuSi_4O_{10}$. The upper inset shows the Schottky heat capacity C_{Sch} and C_p at low temperatures; solid lines are fits to Eqs. (4) and (6). The lower inset shows the entropy of Schottky anomaly and of the transition at 103 K. There is a break on the x-axis separating two different temperature ranges.

atypical of crystalline insulators for which an increasing κ with decreasing T toward a low-T maximum is the signature of phonon transport with mean-free path (mfp) limited by anharmonic decay (phonon–phonon scattering), i.e. mfp $\propto 1/T$ at high T. The inset of Fig. 4 shows the mfp computed for the b-axis data from kinetic theory (mfp $= 3\kappa/C_p v$, with v= 3 km/s) and the specific heat C_p data (see below) [26]. Limited to several nm above 40 K, the mfp rises at a much slower rate than $\sim 1/T$ (dashed line in Fig. 4)and then more rapidly below 40 K ($\sim 1/T^{2.7}$). This behavior is reminiscent of that in amorphous materials [27], where the more rapid rise in mfp occurs as the dominant phonon wavelengths exceed the disorder scale. In the present, highly crystalline material, disorder on a few nm scale, is likely associated with low-energy vibrations involving collective motions of the CuO_4 and Si_4O_{10} polyhedral subunits [15].

A feature associated with the structural transition at 103 K is also observed in the heat capacity at constant pressure $C_p(T)$, as shown in Fig. 5. The entropy change of $\Delta S \approx 1.2$ J/mol K associated with the structural transition was determined after the subtraction of the background and it is shown in the lower inset of Fig. 5. No anomaly is evident at the second structural transition at 87 K, within the resolution of our measurements.

For $T \lesssim 2.5$ K, a non-vibrational contribution, superimposed on the vibrational T^3 dependence, starts to emerge. In this region, the heat capacity increases as $1/T^2$ with decreasing T, which is characteristic of the high-T tail of a Schottky anomaly. Measurements to the minimum attainable temperature 0.4 K did not reveal the peak. The Schottky contribution is likely associated with nuclear energy levels because the magnetic interactions between Cu^{2+} ions are negligible in the Han Blue, but other effects such as magnetic dipolar interactions may be taking place. Since only data for the high temperature side of the Schottky peak was obtained, it is difficult to determine how many energy levels the system possesses. Therefore, a simplified analysis was made using the Schottky heat capacity (C_{Sch}) and entropy (S_{Sch}) for a two-level system [28]:

$$C_{Sch} = R\left(\frac{\delta}{T}\right)^2 \frac{\exp(\delta/T)}{[1+\exp(\delta/T)]^2}, \quad (4)$$

and

$$S_{Sch} = R\left\{\ln[1 + \exp(\delta/T)] + \frac{\delta/T}{1 + \exp(\delta/T)}\right\}, \quad (5)$$

where $\delta = (\epsilon_1 - \epsilon_0)/k_B$ is the energy separation between levels divided by k_B, the Boltzmann constant, and R the gas constant. The fitting of Eq. (4) to the experimental $C_{Sch}(T)$ is shown in the upper inset of Fig. 5, where C_{Sch} was obtained by subtracting the lattice contribution from C_p. We obtained $\delta = 0.28$ K from the fitting and this value was used in Eq. (5) to calculate S_{Sch} that is shown in the lower inset of Fig. 5. $S_{Sch} = 5.75$ J/(mol K), which corresponds to the expected $R\ln(2)$ value for the two-level case.

The heat capacity data was also used to extract the Debye temperature and the Grüneisen parameters. The Debye temperature can be determined by fitting [28]

$$C_v = 9rR\left(\frac{T}{\Theta_D}\right)^3 \int_0^{\Theta_D/T} \frac{x^4 e^x}{(e^x - 1)^2}\, dx, \quad (6)$$

to the experimental data, where r is the number of atoms per formula unit, R the gas constant, T the temperature, and Θ_D the Debye temperature. The relation between heat capacity at constant pressure C_p and volume C_v is given by

$$C_v = C_p - \frac{TV\Omega^2}{X_T}, \quad (7)$$

where V is the molar volume, Ω the volume thermal-expansion coefficient, and X_T the isothermal volume compressibility. Estimates using Eq. (7) and X_T from Ref. [14] reveal that $C_v = 0.99C_p$, as a result, we take $C_p \approx C_v$ for $T \leq 300$ K. Attempts to fit the data with the Debye model over the entire temperature range above 3 K were unsuccessful. Fitting was only possible in the range 3 K $\leq T \leq$ 15 K, (see the upper inset of Fig. 5, solid line) which resulted in a Debye temperature of ≈265 K. Since C_p does not follow the Debye model for $T > 15$ K, this implies that the Debye T^3 law applies only in the limit of low T or long wave-length.

The Grüneisen tensor γ_λ for anisotropic solids is given by [24,29]

$$\gamma_\lambda = \frac{V}{C_v}\sum_\nu c_{\lambda\nu}\mu_\nu, \quad (8)$$

where V is the molar volume, C_v the heat capacity, $c_{\lambda\nu}$ the elastic stiffness, and μ_ν the linear thermal-expansion coefficient. The indices λ and ν take on the values 1–6. For a tetragonal structure, the principal Grüneisen functions are reduced to

$$\gamma_1 = \frac{V[(c_{11} + c_{12})\mu_1 + c_{13}\mu_3]}{C_v}, \quad (9)$$

and

$$\gamma_3 = \frac{V(2c_{13}\mu_1 + c_{33}\mu_3)}{C_v}, \quad (10)$$

where μ_1 and μ_3 are linear thermal-expansion coefficients perpendicular and parallel to the c-axis, respectively. The volumetric Grüneisen function for anisotropic crystal is given by

$$\gamma = \frac{\Omega V}{X_T C_v}, \quad (11)$$

or

$$\gamma = \frac{2X_1\gamma_1 + X_3\gamma_3}{X_T}, \quad (12)$$

where X_1 and X_3 are the isothermal axial compressibility within the plane and along the c-axis, respectively. The Grüneisen parameters determined by using the elastic constant from Ref. [14], and the present heat capacity and thermal expansion data, are $\gamma_1 = -1.09$, $\gamma_3 = 1.06$ and $\gamma = 0.10$ at room temperature. The Grüneisen parameters were determined at room temperature because of the availability of elastic properties only at this temperature. They are expected to be temperature dependent because of the high anisotropy of Han Blue [28]. Although the Han Blue structure possesses higher complexity than graphite [24,28], their anisotropic properties can still be compared. They both have their largest thermal expansions along c, negative thermal expansions within the plane, and positive and negative Grüneisen parameters parallel and perpendicular to c, respectively.

4. Conclusion

High-resolution thermal-expansion measurements reveal two structural phase transitions in Han Blue at 87 K and 103 K that lead to, possibly, two reductions in crystallographic symmetry from the tetragonal structure that exists for $T >$ 103 K. Although it is impossible for our measurements to determine the new crystal structure(s), they provide the temperatures of the transitions as well as the resolution required to observe them, which will serve as a guide in the event that diffraction measurements are pursued. Heat capacity data reveal evidence only for the structural phase transition at 103 K and thermal conductivity reveals features at both transitions. Highly anisotropic thermal expansion, negative thermal expansion perpendicular to the c direction, and negative volume thermal expansion were observed. The heat capacity obeys the Debye-T^3 law only below 15 K. Grüneisen parameters at room temperature are consistent with the highly anisotropic nature of Han Blue. The negative thermal expansion, unusual behavior of the thermal conductivity and heat capacity, and the Grüneisen parameters are consistent with the presence of low-energy vibrations associated with the collective motions of the CuO_4 and Si_4O_{10} polyhedral subunits.

Acknowledgements

Work at Montana State University was supported by CNPq-Brazil under Grant no. 237050/2012-9 and the National Science Foundation under Contract no. DMR-0907036. Work at the University of Miami was supported by the U.S. Department of Energy (DOE), Office of Science, Basic Energy Sciences (BES) under Award no. DE-FG02-12ER46888.

References

[1] E.W. FitzHugh, L.A. Zycherman, A purple Barium Copper Silicate pigment from early China, Stud. Conserv. 37 (3) (1992) 145–154.
[2] H. Berke, Chemistry in ancient times: the development of blue and purple pigments, Angew. Chem. Int. Ed. 41 (14) (2002) 2483–2487.
[3] S.M. Borisov, I. Klimant, A versatile approach for ratiometric time-resolved read-out of colorimetric chemosensors using broadband phosphors as secondary emitters, Anal. Chim. Acta 787 (0) (2013) 219–225.
[4] S.M. Borisov, C. Würth, U. Resch-Genger, I. Klimant, New life of ancient pigments: application in high-performance optical sensing materials, Anal. Chem. 85 (19) (2013) 9371–9377.
[5] G. Pozza, D. Ajò, G. Chiari, F.D. Zuane, M. Favaro, Photoluminescence of the inorganic pigments Egyptian Blue, Han Blue and Han Purple, J. Cult. Herit. 1 (4) (2000) 393–398.
[6] A. Pabst, Structures of some tetragonal sheet silicates, Acta Crystallogr. 12 (10) (1959) 733–739.
[7] V.V. Mazurenko, M.V. Valentyuk, R. Stern, A.A. Tsirlin, Nonfrustrated interlayer order and its relevance to the Bose–Einstein condensation of magnons in $BaCuSi_2O_6$, Phys. Rev. Lett. 112 (2014) 107202.
[8] R. Stern, I. Heinmaa, E. Joon, A.A. Tsirlin, H. Nakamura, T. Kimura, Low-temperature high-resolution solid-state (cryoMAS) NMR of Han purple $BaCuSi_2O_6$, Appl. Magn. Reson. 45 (11) (2014) 1253–1260.

[9] M. Jaime, V.F. Correa, N. Harrison, C.D. Batista, N. Kawashima, Y. Kazuma, G. A. Jorge, R. Stern, I. Heinmaa, S.A. Zvyagin, Y. Sasago, K. Uchinokura, Magnetic-field-induced condensation of triplons in Han purple pigment $BaCuSi_2O_6$, Phys. Rev. Lett. 93 (2004) 087203.
[10] J. Janczak, R. Kubiak, Refinement of the structure of Barium Copper Silicate $BaCu[Si_4O_{10}]$ at 300 K, Acta Crystallogr. Sect. C 48 (7) (1992) 1299–1301.
[11] G. Giester, B. Rieck, Effenbergerite, $BaCu[Si_4O_{10}]$, a new mineral from the Kalahari Manganese field, South Africa: description and crystal structure, Miner. Mag. 58 (1994) 663–670.
[12] E. Kendrick, C.J. Kirk, S.E. Dann, Structure and colour properties in the Egyptian blue family, $M_{1-x}M'_xCuSi_4O_{10}$, as a function of M, M′ where M, M′ = Ca, Sr and Ba, Dyes Pigments 73 (1) (2007) 13–18.
[13] L. Chuanyi, Electronic structures of square planar coordinated transition metal ions in compounds with Gillespite structure, Chin. J. Geochem. 9 (1990) 132–136.
[14] A. Tröster, W. Schranz, R. Miletich, How to couple Landau theory to an equation of state, Phys. Rev. Lett. 88 (2002) 055503.
[15] K.S. Knight, C.M.B. Henderson, Structural basis for the anomalous low-temperature thermal expansion behaviour of the Gillespite-structured phase $Ba_{0.5}Sr_{0.5}CuSi_4O_{10}$, Eur. J. Miner. 19 (2) (2007) 189–200.
[16] J.J. Neumeier, R.K. Bollinger, G.E. Timmins, C.R. Lane, R.D. Krogstad, J. Macaluso, Capacitive-based dilatometer cell constructed of fused quartz for measuring the thermal expansion of solids, Rev. Sci. Instrum. 79 (3) (2008) 033903.
[17] R.L. Carlin, Magnetochemistry, Springer-Verlag, Berlin, 1986.
[18] K.-H. Hellwege, A.M. Hellwege, Landolt–Börnstein, New Series II/16, 1986, Springer-Verlag, Heidelberg
[19] J.S. Griffith, The Theory of Transition-Metal Ions, Cambridge University Press, Cambridge, 2009.
[20] D.R. Lide, CRC Handbook of Chemistry and Physics, CRC Press, Boca Raton, FL, USA, 2002.
[21] A.B. Pippard, The Elements of Classical Thermodynamics, Cambridge University Press, London, 1961.
[22] K.M. Manu, P.S. Anjana, M.T. Sebastian, Low permittivity $SrCuSi_4O_{10}$-LMZBS glass composite for LRCC applications, Mater. Lett. 35 (2011) 565–567.
[23] G. Belenkii, S. Abdullayeva, A. Solodukhin, R. Suleymanov, Peculiarities of thermal-expansion of layered crystals, Solid State Commun. 44 (1982) 1613–1615.
[24] G.D. Barrera, J.A.O. Bruno, T.H.K. Barron, N.L. Allan, Negative thermal expansion, J. Phys.: Condens. Matter 17 (4) (2005) R217–R252.
[25] R.A. Suleimanov, N.A. Abdullaev, The nature of negative linear expansion of Graphite crystals, Carbon 31 (7) (1993) 1011–1013.
[26] R. Berman, Thermal Conduction in Solids, Oxford University Press, Oxford, 1976.
[27] D.G. Cahill, R.O. Pohl, Lattice vibrations and heat transport in crystals and glasses, Ann. Rev. Phys. Chem. 39 (1988) 93–121.
[28] T.H.K. Barron, G.K. White, Heat Capacity and Thermal Expansion at Low Temperatures, Springer Science + Business Media, New York, 1999.
[29] T.H.K. Barron, J.G. Collins, G.K. White, Thermal expansion of solids at low temperatures, Adv. Phys. 29 (4) (1980) 609–703.